THE DEPENDENCE ON OXYGEN FUGACITY
OF NICKEL AND COBALT PARTITIONING
BETWEEN OLIVINE AND SILICATE MELT

by

Deborah A. Zervas

B.S Geology, Indiana University

(1989)

Submitted to the Department of
Earth , Atmospheric, and Planetary Science
In Partial Fulfillment of the Requirements for the
Degree of

MASTER OF SCIENCE

in Geology

at the

Massachusetts Institute of Technology

September 1991

Signature of Author _____

Department of Earth, Atmospheric and Planetary Science
September 11, 1991

Certified by _____

Dr. Timothy L. Grove
Thesis Supervisor

Accepted by _____

Dr. Thomas H. Jordan
Department Head

THE DEPENDENCE ON OXYGEN FUGACITY
OF NICKEL AND COBALT PARTITIONING
BETWEEN OLIVINE AND SILICATE MELT

by

Deborah A. Zervas

ABSTRACT

Experiments in the system olivine-albite-anorthite were conducted to investigate the dependence on oxidation state of nickel and cobalt partitioning between olivine and silicate melt. $D_{Ni}^{oliv/liq}$ and $D_{Co}^{oliv/liq}$ show no dependence on oxygen fugacity at conditions more oxidizing than metal saturation ($-10.3 < \log fO2 < -4.9$, and $-12.2 < \log fO2 < -5.1$ respectively). Upon metal saturation, however, both nickel and cobalt decrease in their affinity for olivine. $D_{Ni}^{oliv/liq}$ drops by a factor of 1.8, from 6.8 to 3.8; $D_{Co}^{oliv/liq}$ similarly drops from 2.8 to 1.65. The change in partitioning behavior may indicate that nickel and cobalt are present in the melt in a mixed valence state.

INTRODUCTION

Nickel partitioning between olivine and silicate melt is a geochemical tool useful for modelling crystallization processes (Hedge 1971, Taylor et al. 1969, Irvine 1974), identifying primary basaltic liquids (Hart and Davis 1978, Clarke and O'Hara 1979) and temperatures of crystallization of basalts (Leemann 1974). The dependence of nickel partitioning on temperature and liquid composition has been thoroughly investigated, early studies examining temperature dependence (Leemann 1974, Mysen 1976, Duke 1976) while later work focussed on separating temperature and compositional effects (Hart and Davis 1978) and on the effect of more chemically complex systems (Kinzler et al. 1990). This study extends previous work by exploring the dependence of nickel partitioning on oxidation state. The experimental results can provide information useful to an understanding of such diverse geologic phenomena as the chemical evolution of planetary interiors and melt structure.

A preliminary study of the dependence of nickel partitioning on oxygen fugacity (Ehlers et al., submitted) shows a step drop in the olivine/liquid partition coefficient for nickel ($D^{ol/liq}_{Ni}$) upon metal saturation. To test the hypothesis that the non-linear change in $D^{ol/liq}_{Ni}$ is due to the presence of Ni^0 in the melt, subsequent experiments on cobalt partitioning were conducted. Ehlers et al. did not observe a step drop in $D^{ol/liq}_{Co}$ over the range in oxygen fugacity covered by the nickel experiments, but metal saturation was not achieved. This study undertakes to expand the range of oxygen fugacity investigated to include saturation with cobalt metal. For the nickel experiments, metal saturation occurred at four log units below the Ni/NiO buffer; the target fO_2 for the cobalt experiments in this study was therefore chosen to be -12.2, four log units below the Co/CoO buffer. An additional nickel experiment was done to better define the point of change in the nickel partition coefficient, given the scatter in the original data.

EXPERIMENTAL PROCEDURES

Starting Materials

A powder mix similar in composition to that of a barred olivine chondrule from an ordinary chondrite (Lux et al. 1981) was synthesized from end member components Fo_{86} (67.49%), Ab (27.03%), and a pseudo-An (5.48%), after Ehlers et al. (submitted) and Kinzler et al. (1990). The Fo, Fa, and pseudo-An components were synthesized from Johnson Matthey high purity oxides as reported in Kinzler et al. (1990). The pseudo-An component incorporates 35% more CaO than stoichiometric anorthite plagioclase in order to maintain a non-plagioclase (i.e. basaltic) liquid composition (Watson 1977). Powdered Amelia albite was used for the Ab component to reduce Na_2O volatilization (Kinzler et al. 1990). Addition of sodium as crystalline plagioclase is thought to enhance the formation of a plagioclase-like structural component in the melt that inhibits the release of sodium to furnace gas. The trace elements Co and Ni were added as oxides to the synthetic chondrule mix in amounts equal to 1-2% of total weight. All mixes were ground under alcohol for 4-6 hours in an agate mortar and pestle.

CONTAINERS

In order to circumvent problems posed by Fe-Mg exchange with containers, crucibles fashioned from San Carlos olivine were used, as in Ehlers et al. (submitted). San Carlos olivine is of the composition Fo_{89-91} and will be in equilbrium with the Fo_{90} olivine and melt assemblage generated by the synthetic chondrule starting composition at 1350°C. Roughly cubic individual crucibles were cut from single crystal San Carlos olivine, and cored in the center of one face. The holes, 4mm in diameter and 5mm deep, serve as repositories for the powder charges. After being packed with 40-50 mg of powder

the crucibles were wrapped and hung on the furnace assembly with platinum wire. At no time is platinum in contact with powder or melt.

RUN CONDITIONS

All experiments were run in a 1 atm Deltech DT31VT gas mixing furnace at 1350°C ± °C. Temperature was monitored with Pt-$Pt_{90}Rh_{10}$ thermocouples that have been calibrated against the melting points of NaCl, Au, and Pd on the IPTS 1968 (Biggar, 1972).

Oxygen fugacities were maintained by mixtures of H_2 and CO_2 supplied at a low flow rate of ~0.1 ml/s that minimizes Na loss (Tormey et al., 1987). A ZrO_2- CaO electrolyte cell positioned in the furnace hot spot was used to monitor oxygen fugacity. The oxygen cell was calibrated at the Fe/FeO and Cu/Cu_2O buffers using values from Huebner (1971).

All experiments were quenched in water to preserve assemblages existing at run conditions.

ANALYTICAL METHODS

Chemical analyses of run products were performed on a four spectrometer JEOL model 733 electron microprobe at an accelerating potential of 15 keV. The silicate data were collected using wavelength dispersive spectrometers and Tracor Northern 5500-5600 automation. Sample current for the nickel experiments was 30 nA for all elements; for the cobalt experiments sample current was 200 nA for cobalt analyses and 10nA for all other elements. Electron beam spot size was 2 microns for olivine analyses and 10 microns for glass analyses of the nickel experiments. For the olivine analyses of cobalt, beam size broadened to 5 microns because of the high sample current. Due to the low detectability of cobalt and nickel, especially in metal saturated experiments, count times were increased

5

over those usual for major element analysis. Cobalt was counted for 250 seconds, nickel for 60 seconds, and all other elements for between 10-40 seconds. Minimum detectability limits are shown in Table 1. For nickel experiments, counting statistic uncertainties (1 sigma) are less than .7% for major elements (Al, Fe, Si, Mg) less than 2.0% for minor elements (Ca, Na), and less than 6.5% for nickel in the glass; in olivine counting statistic uncertainties are less than .7% for major elements (Fe, Si, Mg), less than 22.0% for minor elements (Ca, Al), and less than 1.6% for nickel. Cobalt experiment counting statistic uncertainties are similar to those obtained in the analyses of nickel experiments for major and minor elements, and less than .5% for cobalt in both olivine and glass.

Standards used for most elements are the same as those reported in Kinzler et al. 1990, and are listed in Table 1. Co-olivine was used as the standard for cobalt analysis.

The silicate and metal data were reduced using the correction scheme of Bence and Albee (1968). As discussed in Kinzler et al. (1990) and Ehlers et al. (submitted), this correction scheme gives the same result as conventional ZAF procedures. Analytical uncertainties (1 sigma) are 1.2% (glass) and 2.4% (olivine) for cobalt experiments, larger than counting statistics, and therefore the dominant source of error. For the nickel experiment, counting statistic uncertainties are greater than the analytical uncertainties of 1.2% (glass) and 0.6% (olivine). Longer count times and/or higher beam current for nickel would decrease counting statistic uncertainties to below that of analytical uncertainty. Despite the greater than desired counting statistic errors, the results of the nickel experiment are included here for comparison with previous results. Experimental run conditions along with the run products are given in Table 2; Table 3 presents average analyses for nickel and cobalt experiments along with analytical uncertainties.

In order to minimize excitation of x-rays in the metallic phases present in the metal saturated experiments, and the resultant inaccurate measurement of trace element concentrations, care was taken to analyze regions of olivine and glass that are metal poor. Masking of metal rich regions in metal saturated experiments with carbon paint or a

6

CuTEM grid was shown to be unnecessary for preventing unwanted contributions to trace element concentrations in Ehlers et al. (submitted.)

EQUILIBRIUM

Equilibrium is demonstrated for nickel and cobalt experiments using different criteria. For synthesis nickel experiments, a minimum run time of 48 hours was determined from time temperature equilibration plots calculated by Hart and Davis, 1978. Figure 1 shows their plot recalculated for 95% equilibration. At 1350°C, 48 hours is time enough for a 30 micron diameter olivine sphere to reach equilibrium values, assuming the sphere is immersed in a well mixed reservoir of constant composition. The average length of olivines present in the nickel experiments is 10 microns; no olivine over 30 microns in length was analyzed. The reversal experiments of Kinzler et al. 1990 further support that equilibrium was attained within 48 hours. In that study, synthesis experiments held at one temperature were allowed to re-equilibrate at another. The concentration of nickel in the pre-existing olivines and glass was then compared to the values measured in synthesis experiments conducted only at the final temperature of the re-equilibration experiment. The measured values of the nickel partition coefficient agree within the experimental and analytical uncertainties, and the duration of the synthesis experiments was determined to be sufficient to attain equilibrium.

Equilibrium run times for cobalt experiments were estimated using iron and magnesium interdiffusion coefficients (D) for olivine from Misener (1973) in Figure 2. At 1350°C, -ln D for diffusion along the b axis is equal to 25.3, and D is equal to 1.03 x 10^{-11} cm^2/s. A run time of 48 hours will allow equilibration of a crystal of 26 microns in length, where radial length is equal to the square root of the product of D and time. Iron and magnesium interdiffusion coefficients are appropriate for cobalt diffusion since the

cobalt 2+ ion is intermediate in size between the iron and magnesium ions. The average

length of olivines in the cobalt experiments is 20 microns; no olivine over 30 microns in

length was analyzed. Reversal experiments are necessary to demonstrate that equilibrium

was attained, since partitioning was observed to be dependent on oxidation state.

Loss of major and trace elements from the charges to the containers was

minimized by using San Carlos olivine crucibles. A chemical analysis of San Carlos

olivine shows major element concentrations (iron, magnesium) close to those expected

from olivine in equilibrium with a liquid generated by an olivine chondrule starting

composition at 1350°C (Ehlers et al., submitted). Nickel and cobalt trace element

concentrations are assumed to be similarly in equilibrium with the liquid.

Unexpectedly, orthopyroxene (protoenstatite) is present in two cobalt

experiments, lining the cavity holding the charge (Figure 3). Experiment Co-1 was run at

very reducing conditions (log fO_2 equal to -12.2) for 48 hours, while experiment Co-2 was

run at more oxidizing conditions (log fO_2 at the QFM buffer equal to -3.8), but for an

extended length of time (6 days). Reducing conditions may account for the reaction of the

liquid with the container in experiment Co-1 by changing the composition of the system, as

would sodium loss over time in experiment Co-1. Low oxygen fugacity may precipitate

the reaction by reducing iron in the fayalite component of the melt, releasing oxygen to gas

and effectively increasing the silica content of the melt. In the system quartz-olivine-

diopside-plagioclase, bulk composition moves towards quartz and intersects the

orthopyroxene/olivine reaction curve (Figure 4). Loss of sodium would similarly move

the bulk composition towards quartz . In this case, sodium is a constituent of the albite

component, and loss of sodium releases silica and alumina into the melt.. While the

assemblage of orthopyroxene, olivine, and liquid represents a reaction relation, the three

phase assemblage can be an equilibrium relation for multi-component systems at a constant

temperature, and olivine/liquid partition coefficients for these experiments are valid, albeit

for slightly different starting compositions. In order to monitor the reaction, and determine

8

the time needed for it to go to completion, experiments of duration longer than 48 hours are necessary. Figures 5 and 6 shows magnesium profiles of non-crucible olivines from experiment Co-1(48 hours) and Co-2 (144 hours). Due to a broader electron beam as a result of the high current necessary for statistically valid cobalt counts, and the small size of the olivines grown from the liquid, cobalt profiles of olivine were not possible. Since the cobalt ion is similar in size to the magnesium ion, the olivine is assumed to be similarly homogeneous with respect to cobalt. The olivine profile of Co-1 shows no growth zoning. For experiment Co-2 the greatest difference in MgO content (wt.%) represents ~4% of total MgO. Although this difference is greater than the analytical uncertainty, growth zoning due to compositional changes from sodium loss and consequent orthopyroxene growth is not likely to be the source of such a small variation, but rather small scale heterogeneity of the olivine. Despite sodium loss and the growth of orthopyroxene, olivine crystals are therefore interpreted to be in equilibrium with orthopyroxene and the liquid. Nevertheless, care was taken to analyze adjacent glass and olivine at a distance from orthopyroxene crystals.

As a caveat, it should be noted that homogeneity alone does not guarantee equilibrium (Hart and Davis 1978). Given the slow diffusion in olivine, only minor diffusion may occur at surfaces leaving crystal interiors deceptively unzoned. The partition coefficients measured under such circumstances will be too high. The analytical problems discussed above prevent an accurate characterization of olivine rims, and a question remains as to whether diffusion of cobalt keeps pace with growth of orthopyroxene.

RESULTS

Table 4 presents partition coefficients obtained for the nickel and cobalt experiments. $D^{ol/liq}_{Ni}$ and $D^{ol/liq}_{Co}$ are defined as the weight ratio of NiO and CoO in olivine to NiO or CoO in melt.

9

Experimental results for nickel are presented in two ways. Figure 7 plots $D^{ol/liq}_{Ni}$ against MgO content of the liquid in an effort to discriminate the effects of oxidation state from compositional effects. Included in the plot are data from Ehlers et al. (submitted), Seifert et al. 1988, and Hart and Davis 1978. Significantly, metal saturated experiments define a trend distinct from that of non metal saturated experiments, and suggest a melt structural control on partitioning. A plot of $D^{ol/liq}_{Ni}$ against log fO_2 is shown in Figure 8, where again two trends are in evidence. Metal saturation occurs at log fO_2 equal to -10.3 (Ehlers et al., submitted), and it is at this point that the step drop in $D^{ol/liq}_{Ni}$ is seen. Only those data points from Ehlers et al. (submitted) with starting compositions that correspond to our synthetic olivine chondrule composition are included in Figure 8, in order to eliminate compositional effects that may mask the dependence of $D^{ol/liq}_{Ni}$ on oxidation state.

Experimental results for cobalt are similarly presented in Figures 9 and 10, $D^{ol/liq}_{Co}$ versus MgO content and fO_2 respectively. There is a drop in $D^{ol/liq}_{Co}$ analogous to that in $D^{ol/liq}_{Ni}$ with metal saturation.

DISCUSSION

INTERPRETATION OF RESULTS

The nickel experiment, which is unsaturated with metal, gives a partition coefficient that when plotted against fO_2 along with the data from Ehlers et al. (submitted), follows a trend defined by metal unsaturated experiments that is distinct from the metal saturated trend (Figure 8). This data point more tightly constrains the oxygen fugacity at which the step drop in $D^{ol/liq}_{Ni}$ occurs; a smooth linear variation between the partition coefficients measured at fO_2's corresponding to metal saturation, and those measured at non metal saturated conditions is not predicted. Metal saturation and the associated lower

$D^{ol/liq}_{Ni}$ are projected to occur at an fO_2 between $10^{-9.4}$ and $10^{-10.3}$. While it has been proposed that non-ideality in the olivine solid solution may influence partitioning (Colson 1988), Ehler's et al. (submitted) use an empirical model developed by Kinzler et al. 1990 to account for non-ideality and demonstrate that measured values of $D^{ol/liq}_{Ni}$ are significantly lower than those predicted by equation 4 of Kinzler et al 1990. Ehler's plot is reproduced in Figure 11 with the nickel data point of this study added. Some effect other than non-ideality in the olivine must account for the step drop in $D^{ol/liq}_{Ni}$. Ehler's et al. propose that the valence state of nickel in the melt changes from 2+ to 0 (metallic), thereby reducing the amount of nickel available for incorporation into olivine crystals. The results of the cobalt experiments show a similar change in partitioning behavior upon metal saturation. Given the similarity in the size of the nickel and cobalt ions and their same valence state, it is expected that nickel and cobalt would demonstrate like speciation in the melt.

The question exists as to whether olivine/liquid partition coefficients measured in experiments containing orthopyroxene can be legitmately compared with and included in discussions of those values determined from experiments containing only olivine and liquid. Henry's Law states that activity is independent of concentration. Orthopyroxene, while providing another site option for cobalt and nickel cations, may lower the concentration of trace element in the liquid, but this lower concentration should have no bearing on the partitioning behavior of the element between olivine and melt. Measurements of $D^{ol/liq}_{Co}$ from experiments containing orthopyroxene are therefore included in the results of this study.

IMPLICATIONS

Nickel and cobalt partitioning data can be used to identify the oxidation state of a magma at the time of crystallization of olivine. The lunar basalt measurements of olivine/bulk rock nickel concentration ratios suggest a variable oxidation state for the source

11

region of mare basalts. Chen et al. 1982 analyzed Apollo 14 VLT glasses; a value of 4 for $D_{Ni}^{oliv/liq}$ is calculated from these measurements, indicating metal saturation. Alternatively, high-Ti basalt 74275 analyzed by Delano 1982 gives an approximate $D_{Ni}^{oliv/liq}$ of 10, which suggests non-metal saturated conditions. Cobalt analyses of these and similar rocks could further constrain magmatic oxygen fugacity. Lunar mantle oxidation states in turn are important for understanding lunar formation and constitution.

CONCLUSIONS

Experiments over a range of oxygen fugacity demonstrate a marked change in the partitioning behavior of cobalt and nickel between olivine and silicate melt upon metal saturation. Both nickel and cobalt show a decreased affinity for olivine under reducing conditions, $D_{Ni}^{oliv/liq}$ and $D_{Co}^{oliv/liq}$ dropping by factors of 1.8 and 1.7 respectively. The presence of orthopyroxene, indicating a reaction relation as a consequence of changes in the bulk composition of the system, does not affect the partitioning behavior of the trace metals. The effects of changing oxygen fugacity can be distinguished from compositional effects. The step drop behavior of trace element partition coefficients is interpreted as a consequence of the presence of trace metals in the melt in a mixed valence state, as 2+ ions and 0 charge metals. Similar effects on trace element partitioning may result from other melt speciations. Sulphur, for example, may complex with siderophiles and decrease the amount of 2+ ions available for partitioning. Further measurements of partitioning dependence on oxygen and sulphur fugacity will provide constraints on the volatile budgets of planetary interiors.

REFERENCES

Bence A.E. and Albee A.L. (1968) Empirical correction factors for the microanalysis of silicates and oxides. J. Geol. **76**:382-403

Biggar G.M. (1972) Diopside, lithium metasilicate and the 1968 temperature scale. Mineral. Mag. **38**:768-770

Chen H.-K., Delano J.W. and Lindsley D.H. (1982) Chemistry and phase relations of VLT glasses from Apollo14 and Apollo 17. Proc. Lunar Planet Sci. 13th, A171-A181.

Clarke D.B. and O'Hara M.J. (1979) Nickel, and the Existence of High-MgO Liquids in Nature. Earth Planet. Sci. Lett. **44**:153-158

Delano J.W. (1982) Chromium, nickel and titanium abundances in 74275 olivines: more evidence for a high pressure origin og high-titanium basalts. Lunar Planet. Sci., XIII, p.160-161.

Duke J.M. (1976) Distribution of the period four transition elements among olivine, calcic clinopyroxene and mafic silicate liquid: experimental results. J.Petrol. **17**:499-521.

Ehlers K., Sisson T.W., Recca S.I. and Grove T.L. The effect of oxygen fugacity on the partitioning of nickel and cobalt between olivine, silicate melt and metal. Submitted to Geochim. Cosmochim. Acta.

Hart S.R. and Dacis K.E. (1978) Nickel partitioning between olivine and silicate melt. Earth Planet. Sci. Lett. **40**:203-219.

Hedge C.E. (1971) Nickel in high-alumina basalts Geochim. Cosmochim. Acta **33**:522-524

Huebner J.S. (1978) Buffering techniques for hydrostatic systems at elevated pressures. In: <u>Research Techniques for High Temperature and High Pressure</u>, G.C. Ulmer, Ed., Springer, New York, 123-178.

Irvine T.N. (1974) Simple and multiple oxides in magmatic rock systems Carnegie Inst. Washington Yearb. **73**: 300-307.

Kinzler R.J., Grove T.L. and Recca S.I. (1990) An experimental study on the effect of temperature and melt composition on the partitioning of nickel between olivine and silicate melt. Geochim. Cosmochim. Acta **54**:1225-1265.

Leeman W.P. (1974) Petrology of basaltic lavas from the Snake River Plain, Idaho (Part I): Experimental determination of partitioning of divalent cations between olivine and basaltic liquid (PartII). Ph.D Thesis, University of Oregon, 337 pp.

Lux G., Keil K. and Taylor G.C. (1981) Chondrules in H3 chondrites: textures, compositions and origins. Geochim. Cosmochim Acta **45**:675-685

Misener D.J. (1973) Cation diffusion in olivine to 1400°C and 35 kb. In: Geochemical Transport and Kinetics, A.W.Hofmann, B.J. Geletti, N.S.Yoder and R.A.Yund, Eds., Carnegie. Inst. Wash. Publ. **634**:117-125.

Mysen B. (1976) Nickel partitioning between upper mantle crystals and partial melts as a function of pressure, temperature and nickel concentration. Carnegie Inst. Washington Yearb. **75**:662-668.

Seifert S., O'Neill H. St. C. and Brey G. (1988) The partitioning of Fe, Ni, and Co between olivine, metal and basaltic liquid: An experimental and thermodynamic investigation, with application to the composition of the lunar core. Geochim. Cosmochim. Acta **52**:603-616.

Taylor S.R., Kaye M., White A.J.R., Duncan A.R. and Ewart A. (1969) Genetic significance of Co, Cr, Ni, Sc and V content of andesites. Geochim. Cosmochim. Acta **33**:275-286.

Tormey D.R., Grove T.L. and Bryan W.B.(1987). Experimental petrology of normal MORB near the Kane Fracture Zone: 22°-25°N, mid-Atlantic ridge. Contrib. Mineral. Petrol. **96**:121-139.

Watson E.B. (1977) Partitioning of manganese between forsterite and silicate liquid.

Geochim. Cosmochim. Acta **41**:1363-1374.

FIGURE CAPTIONS

Figure 1. Time-temperature equilibration plot for nickel in forsterite. Modified after Hart and Davis (1978). Curves represent conditions necessary for nickel in an olivine sphere to reach 95% of equilibrium value, assuming sphere is immersed in a well-mixed reservoir of constant composition.

Figure 2. Iron-magnesium interdiffusion coefficients. From Misener (1973). Plot shows temperature dependence of D (interdiffusion coefficient) for olivine of composition Fo_{93}. Diffusion will be faster with increasing fayalite component in olivine.

Figure 3. Backscattered electron scanning electron microscope images of cobalt experiments showing the reaction relation of orthopyroxene, olivine, and liquid. Large, dark grey, euhedral crystals are orthopyroxene (opx), smaller light grey, subhedral crystals are olivine (oliv), and light interstitial areas are glass (gl). Metal blebs (m) are evident in the metal saturated experiment. Darkest areas are epoxy. Scale bar is 100 microns. A. Co-1 metal saturated experiment of 48 hour duration. B. Co-2 non-metal saturated experiment of 144 hour duration.

Figure 4. Phase diagram showing change in bulk composition under reducing conditions. Composition moves towards quartz with loss of oxygen to furnace gas as a consequence of the reduction of iron in the fayalite component in the melt, and in the olivine.

Figure 5. Magnesium profile of olivine from metal saturated cobalt experiment Co-1. Magnesium distribution in olivine determined by electron microprobe line scan for an olivine grain. Homogeneity is better than ± 1.5% in olivine. Typical glass analyses adjacent to olivine grain are shown for comparison.

Figure 6. Magnesium profile of olivine from 6 day non-metal saturated experiment Co-2. Magnesium distribution in olivine determined by electron microprobe line scan for an

olivine grain. Homogeneity is better than ± 2.9% in olivine. Typical glass analyses adjacent to olivine grain are shown for comparison.

Figure 7. A comparison of experimentally determined values of $D_{Ni}^{oliv/liq}$ plotted against wt % MgO in the coexisting silicate melt for simple system experiments (Ehlers et al., submitted; Hart and Davis, 1978; Seifert et al., 1988; and this study). Two distinct compositionally dependent trends are evident, one for non-metal saturated experiments (above the line), and one for metal saturated experiments (below the line).

Figure 8. Experimentally determined values of $D_{Ni}^{oliv/liq}$ plotted against log fO_2 (Ehlers et al., and this study). A step drop in $D_{Ni}^{oliv/liq}$ is observed with metal saturation.

Figure 9. Experimentally determined values of $D_{Co}^{oliv/liq}$ plotted against wt. % MgO (Ehlers et al.,, and this study). Value from the metal saturated experiment falls well outside the trend defined by the non-metal saturated experiment.

Figure 10. Experimentally determined values of $D_{Co}^{oliv/liq}$ plotted against log fO_2 (Ehlers et al., and this study). Value from the metal saturated experiment falls well outside the trend defined by the non-metal saturated experiment.

Figure 11. Experimentally determined values of $D_{Ni}^{oliv/liq}$ from Ehlers et al. and this study are plotted against the predicted values of $D_{Ni}^{oliv/liq}$ calculated from equation 4 of Kinzler et al. 1990. The Kinzler et al. expression was derived from partitioning experiments carried out over the range of oxygen fugacities from QFM to air.

Table 1. Standards and minimum detectibility limits

Element	Standard		Minimum detection limit	
	Glass	Olivine	Glass	Olivine
Na_2O	Amelia albite	-	.03	-
MgO	diopside$_{65}$-jadeite$_{35}$	synthetic forsterite	.02	.02
Al_2O_3	diopside$_{65}$-jadeite$_{35}$	diopside$_{65}$-jadeite$_{35}$	.03	.03
SiO2	Shallow water enstatite	synthetic forsterite	.02	.02
CaO	diopside$_{65}$-jadeite$_{35}$	diopside$_{65}$-jadeite$_{35}$	.03	.04
FeO	cossyrite	synthetic fayalite	.04	.04
NiO	P140 olivine	nickel sulfide	.02	.02
CoO	cobalt olivine	cobalt olivine		

Table 2. Experimental conditions and run products

Run	-log fO$_2$	Time (hours)	T (° C)	Run products
Ni-1	9.4	48	1350	oliv, glass
Co-1	12.2	48	1350	oliv, opx, glass
Co-2	6.8	144	1350	oliv, opx, glass

Table 3. Microprobe analyses of run products

3a. Nickel experiments

Expt.	Phase	SiO$_2$	Al$_2$O$_3$	FeO	MgO	CaO	Na$_2$O	NiO	Total
Ni-1	glass	57.51	13.21	9.38	16.49	2.52	1.41	0.192	100.71
		± .08	± .02	±.03	± .03	±..01	±.01	±.002	
	olivine	40.47	0.12	9.45	48.63	0.046	_	1.292	100.01
		± .06	±.05	±.03	± .06	±.002		±.007	

3b. Cobalt experiments

Expt.	Phase	SiO$_2$	Al$_2$O$_3$	FeO	MgO	CaO	Na$_2$O	CoO	Total
Co-1	glass	54.41	15.36	7.47	18.90	3.10	0.252	0.139	99.64
		±.06	±.06	±.02	±.03	±.01	±.009	±.003	
	olivine	41.44	0.043	7.23	51.15	0.043	_	0.314	100.22
		±.07	±.006	±.04	±.16	±.006		±.008	
C0-2	glass	60.74	11.28	8.62	14.35	2.14	2.79	0.584	100.52
		±.14	±.06	±.12	±.07	±.01	± .02	±.014	
	olivine	41.32	0.058	8.13	49.58	0.064	_	1.49	100.64
		±.20	±.003	±.17	±.23	±.004		±.05	

Table 4. Calculated partition coefficients

Run	-log fO_2	Trace element (i)	$D^{oliv/liq}_i$
Ni-1	9.4	nickel	6.73 ± .17
Co-1	12.2	cobalt	1.65 ± .07
Co-2	6.8	cobalt	2.56 ± .05

Figure 1.

Figure 1.

Time (days)

50.0

10.0

5.0

1.0

0.5

0.17

40 microns

30 microns

20 microns

10 microns

1000   1100   1200   1300   1400   1500

T (° C)

Figure 2.

T (°C)

1200   1300   1400

Ln D (cm ^{2}/sec)

C axis

B axis

A axis

24

25

26

27

28

7.0   6.5   6.0

1/T (°K $^{-1}$) x 10 ^{4}

23

Figure 3.

Figure 4.

Qtz

oliv

aug

Oliv

Cpx

Projected from plagioclase
(oxygen units)
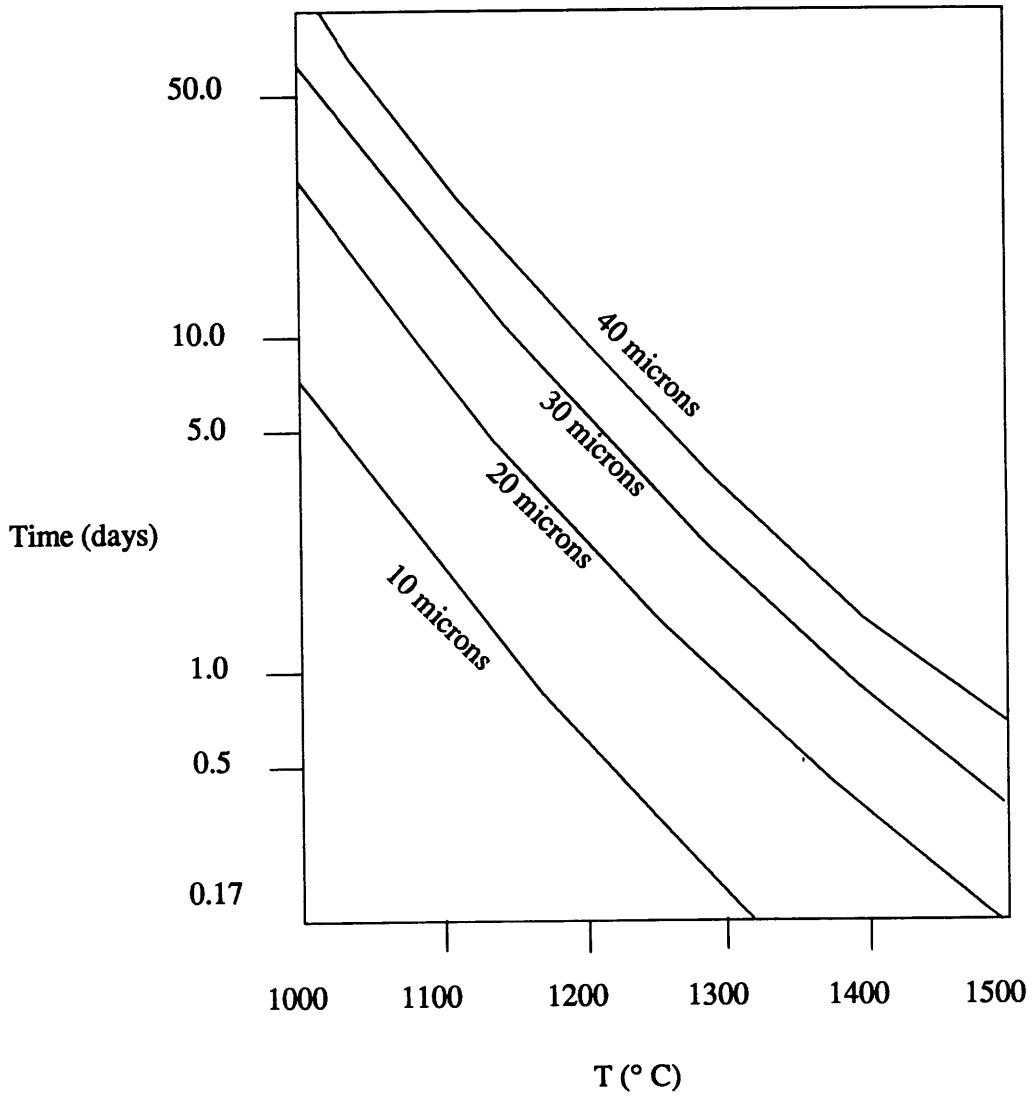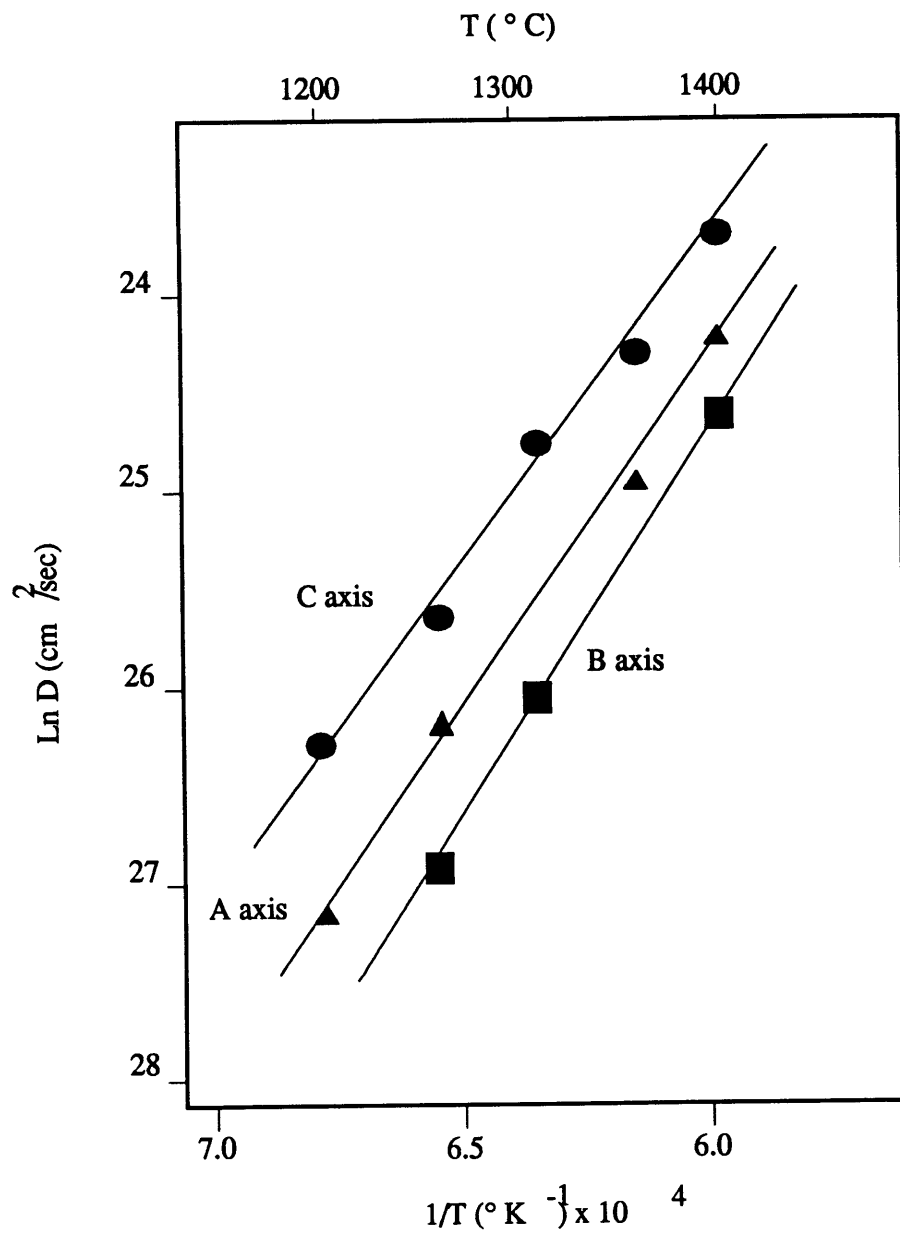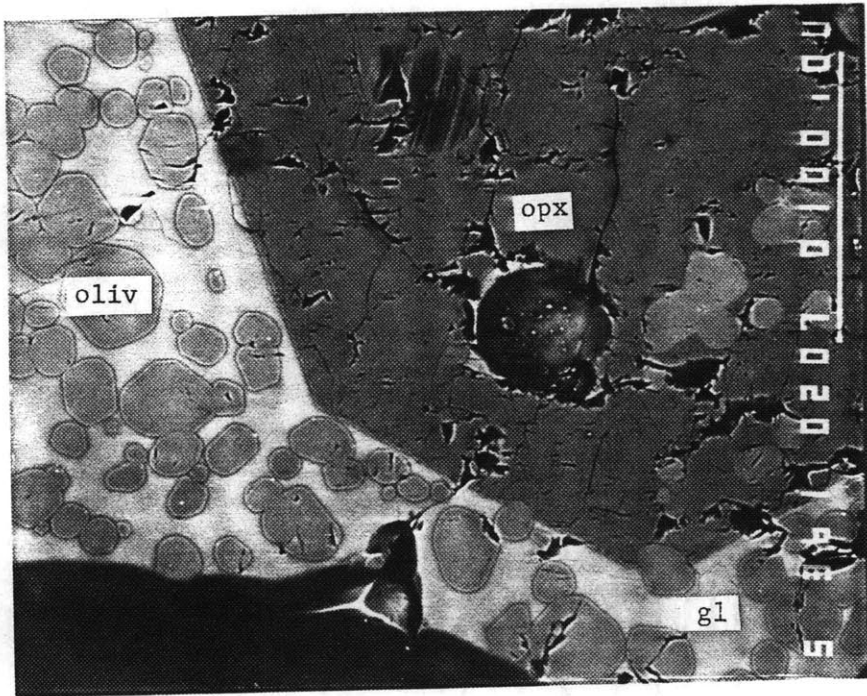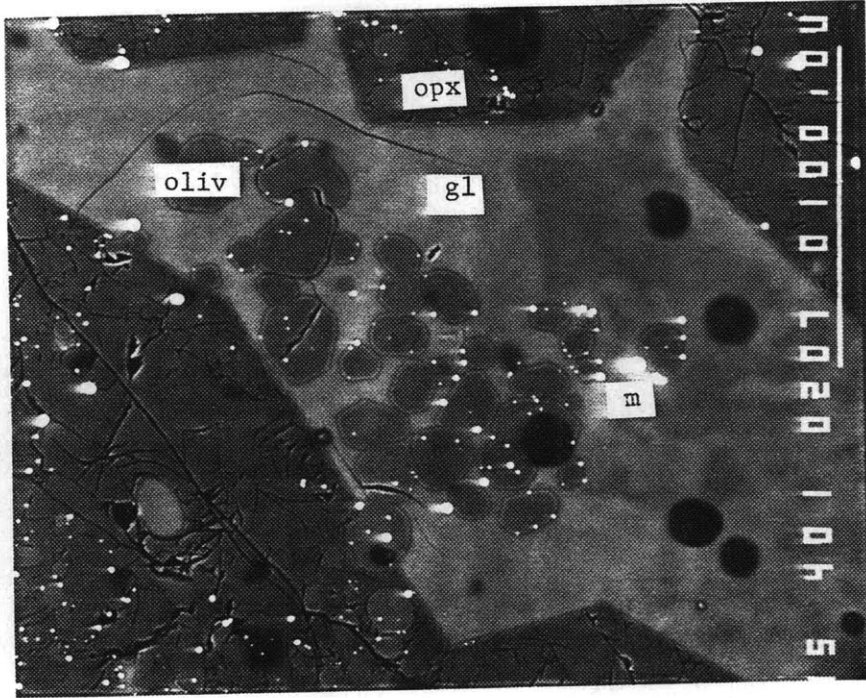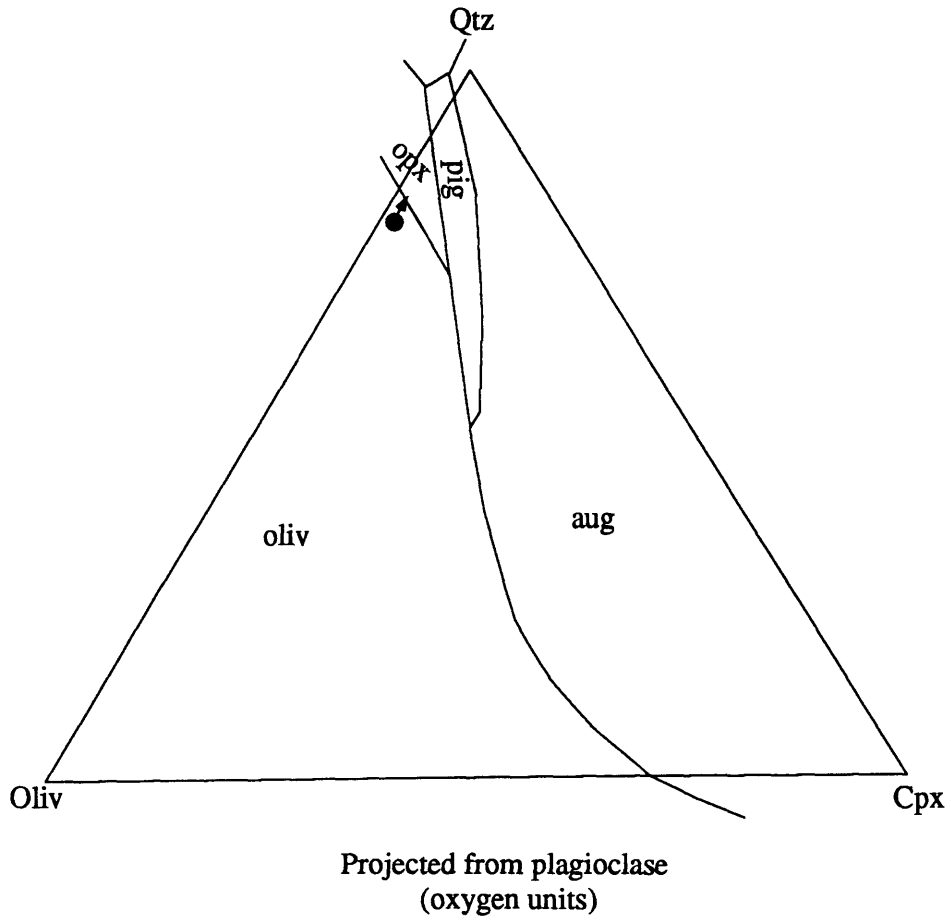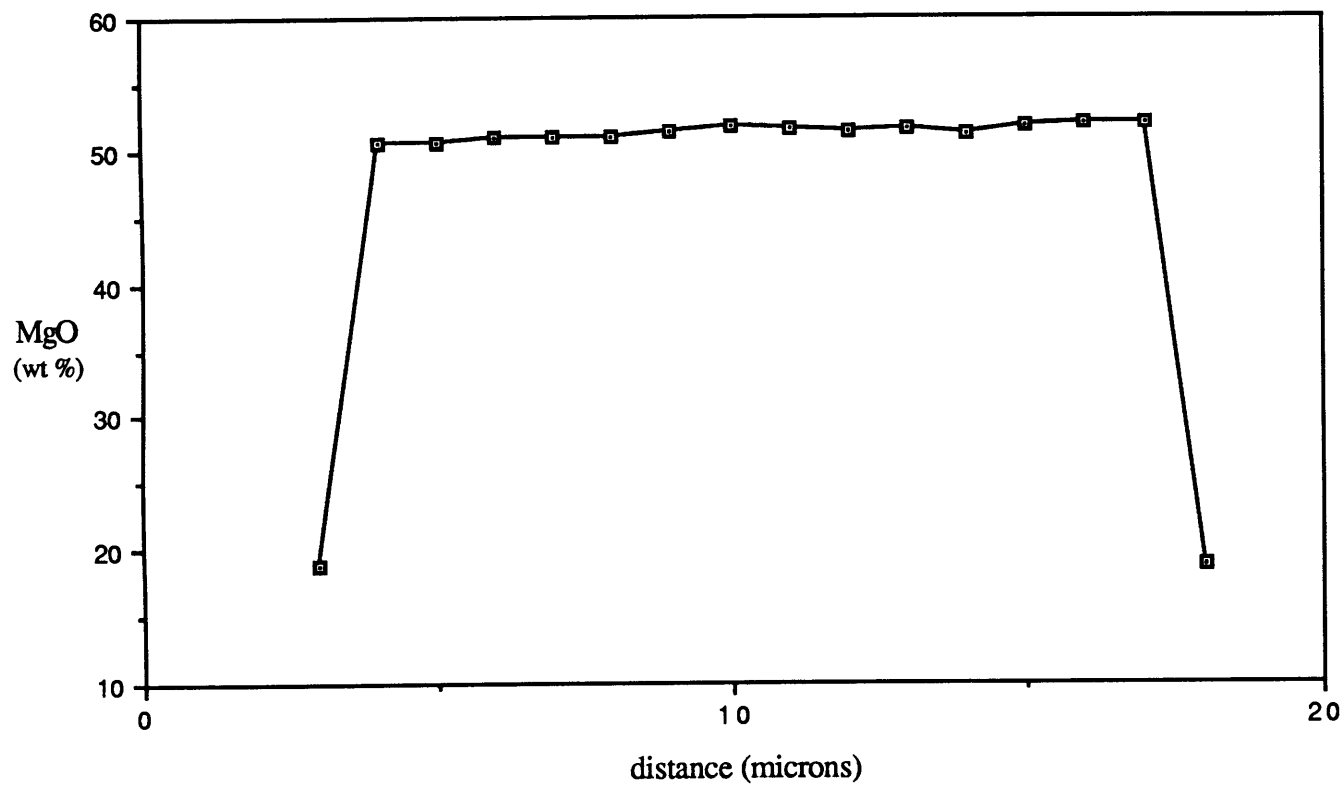
Figure 5.

Figure 6.

Figure 7.

Figure 8.
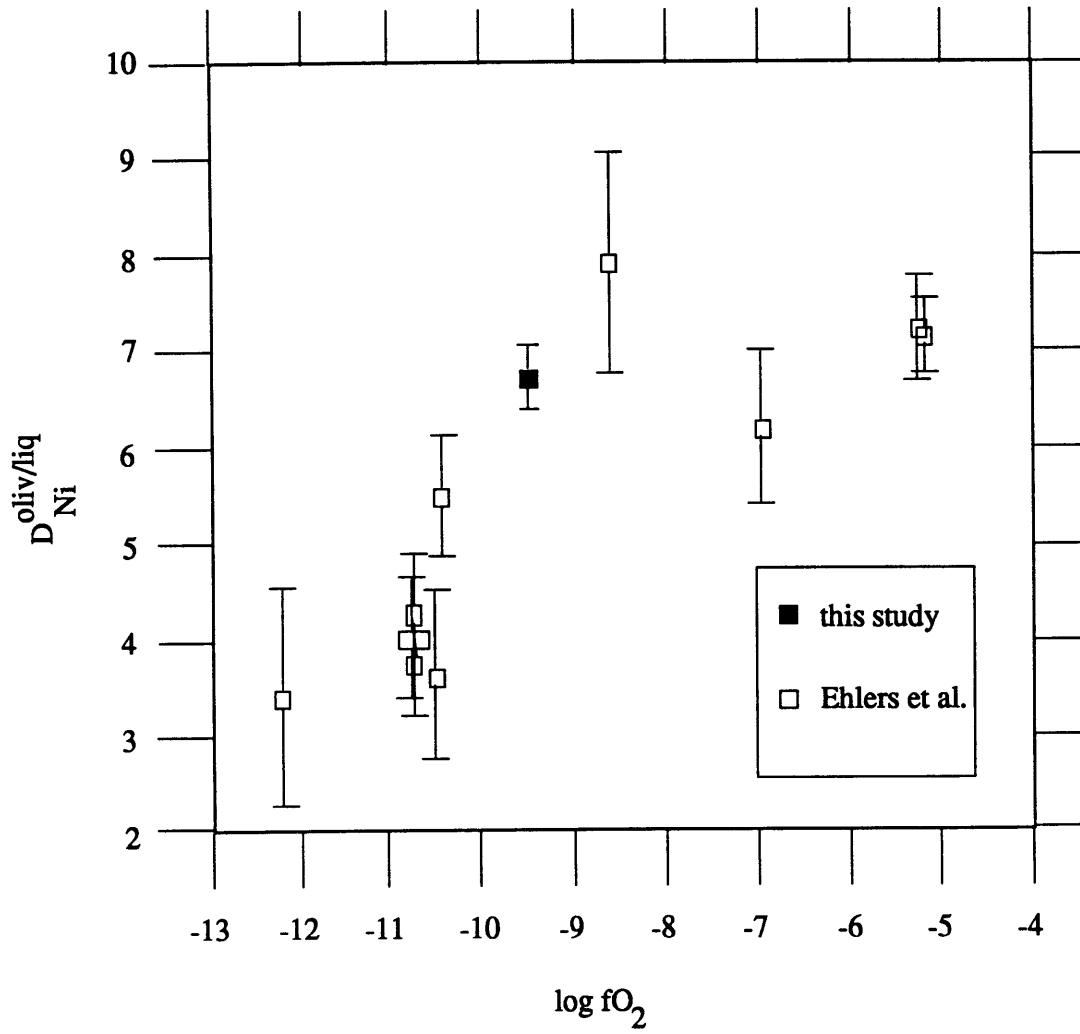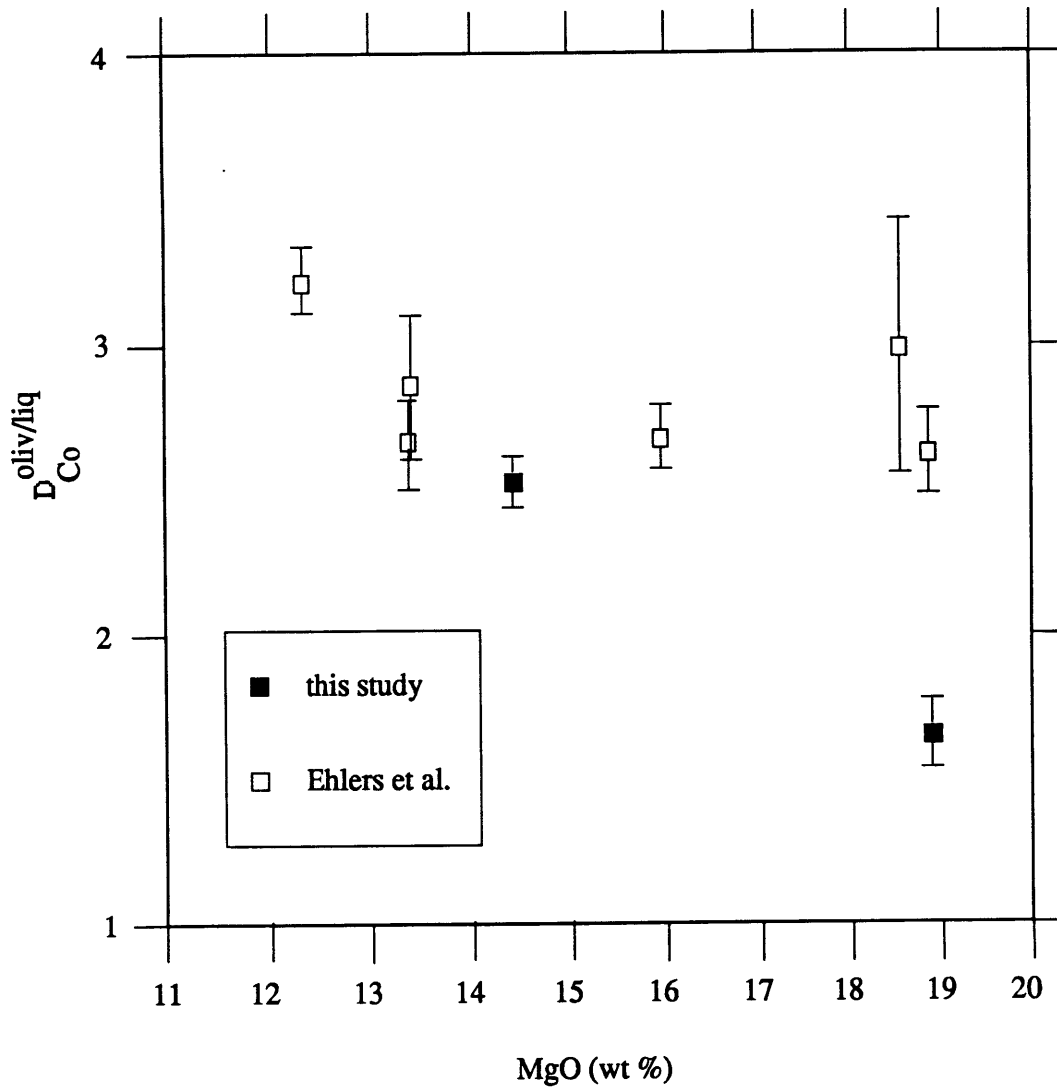

The figure plots $D_{Ni}^{oliv/liq}$ on the vertical axis against $\log fO_2$ on the horizontal axis. Legend: filled square = this study; open square = Ehlers et al.
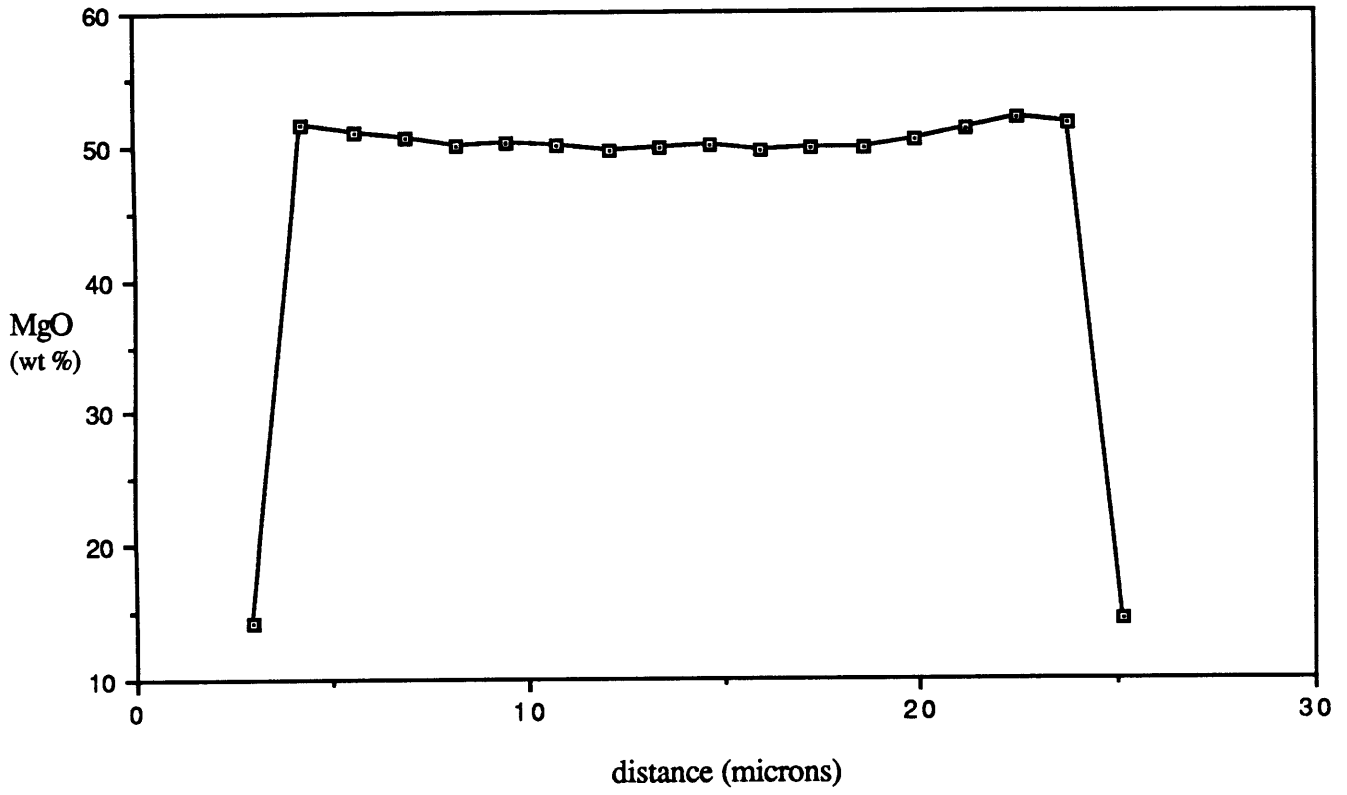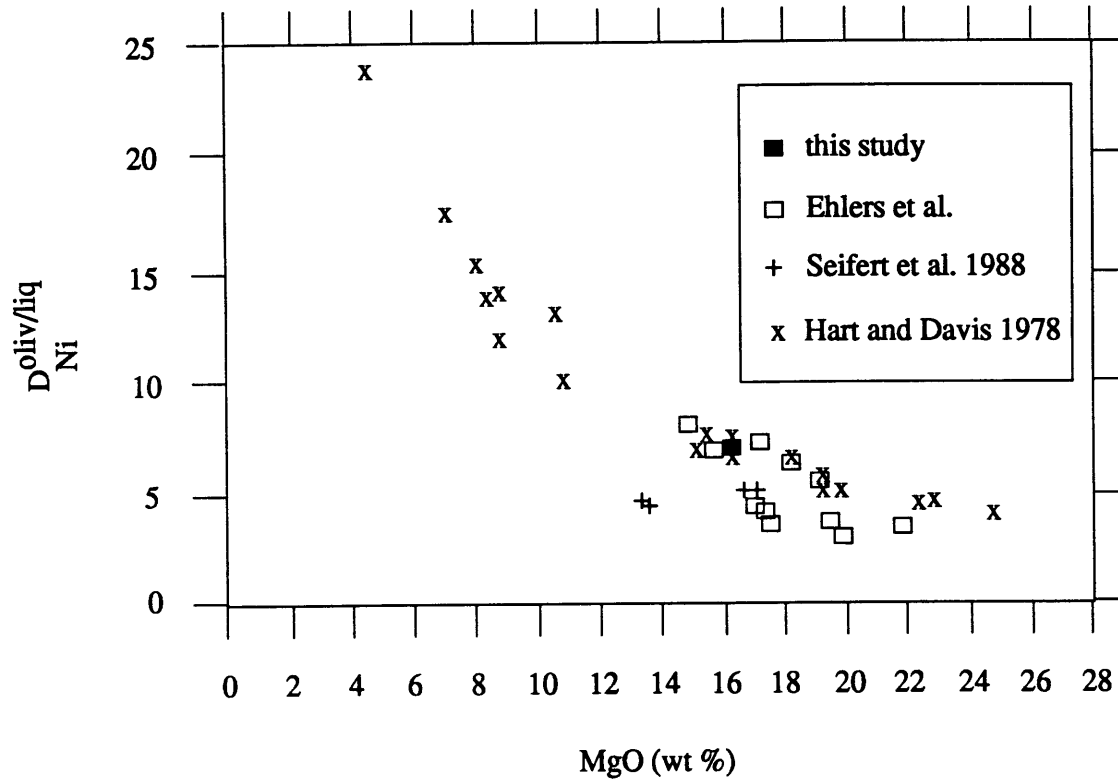
Figure 9.

Figure 10.

Figure 11.